A Comparative Study On The Dynamic Response Of Three Semisubmersible Floating Offshore Wind Turbines

Proceedings of the ASME 2019 38th International Conference on Ocean, Offshore and Arctic Engineering
OMAE2019
June 9-14, 2019, Glasgow, Scotland

OMAE2019-96221

A COMPARATIVE STUDY ON THE DYNAMIC RESPONSE OF THREE SEMISUBMERSIBLE FLOATING OFFSHORE WIND TURBINES

Wei Shi, Lixian Zhang, Dezhi Ning
State Key Laboratory of Coast and Offshore Engineering
Dalian University of Technology
Dalian, China

Zhiyu Jiang
Department of Engineering Sciences
University of Agder
Grimstad, Norway

Constantine Michailides
Department of Civil Engineering and Geomatics
Cyprus University of Technology
Limassol, Cyprus

Madjid Karimirad
Civil Engineering, School of Natural and Built Environment, Queen's University Belfast
Belfast, UK

ABSTRACT

Currently, there is a great interest to globally develop offshore wind energy due to the greenhouse effect and energy crisis. Great efforts have been devoted to develop reliable floating offshore wind energy technology to exploit the wind energy resources in deep seas. This paper presents a comparative study of the dynamic response of three different semisubmersible floating wind turbine structures. All the three platforms support the same 5MW wind turbine. The platforms examined are: a V-shaped Semi, an OC4-DeepCwind Semi and a Braceless Semi at 200 m water depth. A dynamic analysis is carried out in order to calculate and compare the performance of these platforms. The comparison is made on the rigid body motions of the semisubmersible platform and tensions of the mooring lines. The presented comparison is based on statistical values and spectra of the time series of the examined response quantities. Coupling effects are more significant for the V-shaped Semi platform. The V-shaped Semi and the Braceless Semi show a more rational motion response under the investigated load cases. The results of this analysis may help to resolve the fundamental design trade-offs between among different floating system concepts.

INTRODUCTION

Offshore wind energy has experienced rapid development over the past ten years. In 2017, the investment in offshore wind technology in Europe reached up to 7.5 billion Euro. The 560 new offshore wind turbines were connected to the grid with an increased capacity of 3,148 MW [1]. However, most offshore wind turbines are installed in shallow water with bottom-fixed substructures, which includes monopiles, gravity foundations, tripods, tri-piles and jackets that are used in water depths of up to 50 m [2-4]. For greater water depths, the floating offshore wind turbine (FOWT) is a unique solution to harness the offshore wind energy many different countries. Numerous floating platform configurations are possible for use in offshore wind turbines technology, and much has been learned from the knowledge of the offshore oil and gas industry. Based on the fundamental principles adopted to achieve static stability, a floating platform can be classified into three primary concepts: a semisubmersible (Semi), a Spar buoy and a Tension Leg Platform (TLP). Many researchers have made great efforts to investigate the difference in the dynamic responses of a variety of floating wind turbine systems [5−7].

Compared to spar buoys and TLPs, the Semi platforms is more feasible in a variety of water depths and has lower costs of installation. There are several successful semisubmersible floating wind turbine projects over the world, including WindFloat [8], Fukushima FORWARD demonstration project [9] and OO Star Wind Floater [10].

Bayati [11] investigated the impact of second-order hydrodynamics on an OC4-DeepCwind semisubmersible offshore wind turbine. Moreover, the second order hydrodynamic force can stimulate the oscillation of the platform and further cause fatigue damage to the structure. Masciola and Robertson [12] used the coupled and uncoupled models on OC4-DeepCwind semisubmersible FOWT to determine how the mooring systems influence the motion of the FOWT. Luan et al. [13] established a numerical model for a Bracessless semisubmersible platform and performed an extreme sea states analysis. The results showed that the platform has good stability under extreme seas and is a good design concept. Moreover, the

same concept can be used as a combined wind and wave concept with very stable dynamic behavior [14,15]. A 5 MW wind turbine was employed by Kim et al. [16], and the WindFloat and OC4-DeepCwind floating platforms used to focus on the motion of FOWTs and to evaluate the mooring system force by using FAST code [17].

The main objective of the present study is to investigate and compare the responses of three different semisubmersible floating offshore wind turbines including V-shaped Semi, OC4-DeepCwind Semi and Braceless Semi platforms. A dynamic analysis is carried out using ANSYS/AQWA tool (for addressing wave-structure interaction effects) with more emphasis on the hydrodynamic performance of the FOWT system. The present work aims to reveal how the semi platform variation affects the dynamic response of the floating wind turbine system. A comparative study with regards to the dynamic motion of platforms and mooring line tension is carried out to conduct the analysis and draw meaningful conclusions.

THEORY

In this section, the relevant basic theories and approaches for environmental and hydrodynamic loads are discussed.

Equation of Motion

The large volume body is represented by a six degree of freedom (6-DOF) rigid body. The load model for the body accounts for the wind and wave loads. The wind acted on the structure and current forces are based on a set of direction-dependent coefficients for each of the 6-DOF. Both linear and quadratic forces can be included. In this paper, the wind and wave loads are considered, and the structural viscous damping is not included. The equation of motion under wind-wave loads in time domain analysis are calculated in AQWA; for rigid body motion of degree of freedom, j, it can be expressed as:

$$\sum_{i=1}^{6}\left(\left(M_{ij}+A_{ij}\right)\ddot{x}_j(t)+\int_{-\infty}^{t}\dot{x}_j(\tau)K_{ij}\left(t-\tau\right)d\tau+C_{ij}x(t)\right) = F_{wave,j}\left(t\right)+F_{moor,j}\left(t\right)+F_{wind,j}\left(t\right) \quad (1)$$

where M_{ij} is the mass coefficient, A_{ij} is the added mass coefficient calculated with AWQA-LINE, $K_{ij}(t-\tau)$ is the retardation function which represents the fluid memory effect, C_{ij} is the restoring coefficient calculated with AWQA-LINE, $\ddot{\mathrm{x}}$, $\dot{\mathrm{x}}$ and x are the acceleration, velocity, and displacement of the platform, $F_{wave,j}(t)$ is the wave exciting force, $F_{wind,j}(t)$ is the aerodynamic force that acts on the rotor and $F_{moor,j}(t)$ is the restoring force that results from taut mooring lines, j is the degree of freedom (DoF), namely, surge, sway, heave, roll, pitch and yaw.

Wind load

A structure under wind flow will experience static and dynamic wind loads. The wind loads acting on the tower and nacelle are mainly considered as drag forces. However, the wind loads acting on the turbine blades have both lift and drag forces, which can be calculated with the use of different fidelity methods: force-wind speed curve, Blade Element Momentum (BEM), Generalized Dynamic Wake (GDW) or Computational Fluid Dynamics (CFD) [18]. In this paper, the wind load acting on the blades is simplified as a thrust force based on the thrust-wind speed curve of the NREL 5 MW baseline wind turbine [19] (Figure 1).

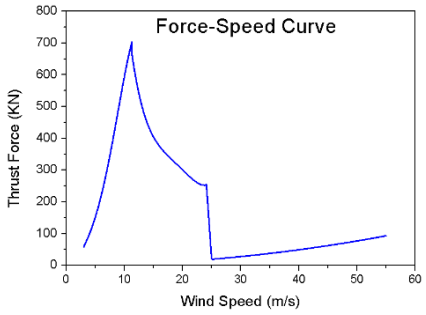

Figure 1. Relation between the mean wind speed and aerodynamic thrust of the NREL 5MW reference wind turbine (reproduced from [18])

Wave load

The hydrodynamic loads can be estimated using Morison's Equation, potential flow theory or higher fidelity numerical modeling techniques (e.g., CFD, SPH) [20]. The Morison's Equation is mainly used to calculate the hydrodynamic loads for slender structures with small diameters when compared with wave length. For large volume structures, diffraction and radiation are relatively important and the potential flow theory is used to calculate the hydrodynamic loads acting on the platform. The potential flow theory considers the solution of a linearized boundary value problem for inviscid and incompressible flow. Only the first-order wave loads are considered in the present study. In potential flow theory, the fluid needs to satisfy Laplace's equation:

$$\nabla^2\phi^{(1)}=\frac{\partial^2\phi}{\partial x^2}+\frac{\partial^2\phi}{\partial y^2}+\frac{\partial^2\phi}{\partial z^2}=0 \quad (2)$$

where $\phi^{(1)}$ is the first order total velocity potential function involving the incident potential $\phi_i^{(1)}$, diffraction potential $\phi_d^{(1)}$, and radiation potential $\phi_r^{(1)}$. To solve the potential function $\phi^{(1)}$ boundary conditions are applied as shown below:

$$\frac{\partial\phi}{\partial z}=0, z=-h \quad (3)$$

$$\frac{\partial^2\phi}{\partial t^2}+g\frac{\partial\phi}{\partial z}=0, z=0 \quad (4)$$

$$\frac{\partial\phi}{\partial n}=\sum_{i=1}^{n}v_i f_i\left(x,y,z\right) \quad (5)$$

$$\lim_{R\to\infty}\phi=0 \tag{6}$$

Once $\phi^{(1)}$ is solved, the exciting wave forces and moment can be obtained by integration over the wetted body surface.

$$F_{EXj}^{(1)} = \mathrm{Re}\left\{-\rho A e^{iwt}\iint_S n_j\left(\phi_i+\phi_d\right)dS\right\}, j=1,2,3$$
$$M_{EXj}^{(1)} = \mathrm{Re}\left\{-\rho A e^{iwt}\iint_S \left(r\times n\right)_j\left(\phi_i+\phi_d\right)dS\right\}, j=4,5,6 \tag{7}$$

Where: S is the wetted surface of the platfrom, A is the wave amplitude.

MODEL DEVELOPMENT OF THE SEMISUBMERSIBLE FOWTS

Wind Turbine Model

The wind turbine used in this paper was developed by the National Renewable Energy Laboratory (NREL) in the USA [18]. It is a conventional three-bladed, upwind, variable speed, collective-pitch controlled horizontal axis wind turbine. The main properties of the turbine for the wind speed and the mass distribution are listed in Table 1. Detailed information can be found in [19].

Table 1. Main properties of NREL 5 MW baseline OWT [19]

Parameter	Value
Rated power	5 MW
Rotor Orientation	Upwind
Rotor, Hub Diameter	126 m, 3m
Hub height	90 m
Cut-In, Rated, Cut-Out Wind Speed	3.0 m/s, 11.4 m/s, 25.0 m/s
Cut-In, Rated Rotor Speed	6.9 rpm, 12.1 rpm
Overhang, Shaft tilt, Precone	5 m, 5°, 2.5°
Rotor, Nacelle, Tower mass	110 t, 240 t, 347.46 t
Tower top, diameter, wall thickness	3.87 m, 0.019 m

Semisubmersible platform model

The systems modeled include three different semi platforms: V-shaped Semi, OC4-DeepCwind Semi and Braceless Semi. All of these floating platforms were developed to support the rotor, nacelle, and tower of the NREL 5-MW reference wind turbine. The water depth is assumed to be 200 m. The systems are illustrated in Figure 2 and their properties are summarized in Table 2. As can be found from Table 2, the displacement of the OC4-DeepCwind Semi is much larger than the displacement of the V-shaped Semi (39%) and the Braceless Semi (32%). The numerical model of the three platforms was simulated in ANSYS/AQWA. The element length of the panel model is 0.3 m, and the mapped mesh is used in order to reduce calculation errors, avoid divergence and obtain more accurate results.

The V-shaped Semi platform is mainly composed by a center column and two side columns connected by two pontoons to the center column. The NREL 5 MW wind turbine's tower is located at the top of the center column. The global coordinate system is built on the center column. Detailed information for the original design is available in [21- 23].

The OC4-DeepCwind Semi is mainly composed of a central column and three outer offset columns. It has heave plates (base columns) which are attached to the bottom of the upper columns in order to prevent large heave motions of the platform. Several slender bracings are also used as a connection between the columns and make the platform structure stiff. More details can be found in [24]. To make the arrangement of columns and the mooring line configuration comparable to the other platforms, the OC4-DeepCwind Semi platform in this paper was rotated 180 degrees from its original design.

The Braceless Semi consists of three pontoons, three side columns and one central column supporting the tower and the wind turbine. The global coordinate system is built on the center column. Detailed information is available for the Braceless Semi in [13].

The mooring system of the three floating platforms is composed of three catenary chain mooring lines. The chain mooring lines are simplified as a uniformly distributed mass with a solid circle cross-section. The clump mass of the V-shaped Semi is positioned 100 m from the fairlead of each mooring line, while the clump mass of each mooring line in the Braceless Semi is positioned 240 m far from the fairlead position. More detailed parameters of the mooring system are described in Table 3.

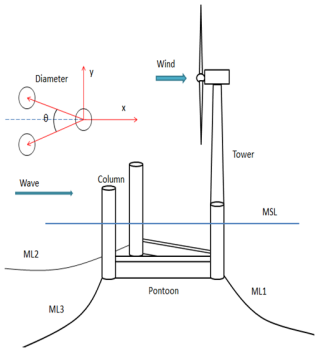

(a) V-shaped Semi

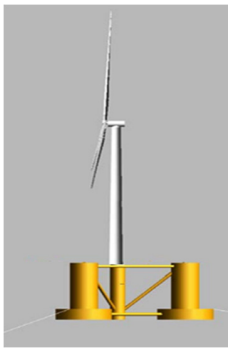

(b) OC4-DeepCwind Semi

(c) Bracessless Semi

Figure 2. Semisubmersible floating wind turbine concepts

Table 2. Properties for the three semisubmersible floating platforms

Parameter	V-shaped Semi	OC4-DeepCwind Semi	Bracessless Semi
Water depth/m	200.0	200.0	200.0
Freeboard/m	20.0	12.0	20.0
Draft/m	28.0	20.0	30.0
Submerged volume/ m^3	10,013	13,917	10,517
Floater steel mass/kg	1,630,000	3,852,000	1,686,000
Total mass/kg (Including WT, Mooring lines)	10,300,000	14,070,000	10,780,000
COG (x,y,z)/m	(-30.6, 0.0, -16.0)	(0.0, 0.0, -9.9)	(0.0, 0.0, -18.9)
I_{xx} w.r.t. COG /kg*m^2	12,900,000,000	10,110,000,000	10,650,000,000
I_{yy} w.r.t. COG /kg*m^2	21,800,000,000	10,110,000,000	10,650,000,000
I_{zz} w.r.t. COG /kg*m^2	17,900,000,000	12,779,000,000	8,412,000,000

Table 3. Properties of mooring line system

Parameter	V-shaped Semi	OC4-DeepCwind Semi	Bracessless Semi
Mooring line length/m	700.0	835.5	700.0
Number of mooring lines	3	3	3
Mass per unit length/kg/m	117.0	108.6	115.0
Diameter of mooring line/m	0.1380	0.0766	0.1370
Fairlead for ML1 (x,y,z)/m	(4.5, 0.0, -18.0)	(40.9, 0.0, -14.0)	(43, 0.0, -18.0)
Fairlead for ML2 (x,y,z)/m	(-55.8, -32.3, -18.0)	(837.6, 0.0, -200.0)	(-22.1, 38.3, -18.0)
Fairlead for ML3 (x, y,z)/m	(-55.8, 32.3, -18.0)	(-20.4, -35.4, -14.0)	(-22.1, -38.3, -18.0)
Anchor point of ML1 (x, y, z)/m	(650.0, 0.0, -200.0)	(-418.8, -725.4, -200.0)	(1084.4, 0.0, -200.0)
Anchor point of ML2 (x, y, z)/m	(-618.7, -357.0, -200.0)	(-20.4, 35.4, -14.0)	(-542.2, 939.1, -200.0)
Anchor point of ML3 (x, y, z)/m	(-618.7, 357.0, -200.0)	(-418.8, -725.4, -200.0)	(-542.2, -939.1, -200.0)
Clump mass volume/m^3	4.4	-	-
Clump mass weight/kg	37,000	-	40,000
Placement of clump mass from fairlead/m	100.0	-	240.0

RESULTS AND DISCUSSION

Natural frequency of three platforms

It must be noted that during the analysis the motions of the platforms are coupled. However, it is possible to initially assume that the motions are uncoupled in order to investigate the natural frequencies of the system by empirical formulas (heave, roll and pitch motion) that in most cases provide a good approximate estimation of the natural frequencies of the system. Based on the decay test and dynamic analysis, the natural frequencies of the three floating platforms are illustrated in Table 5.

$$\omega = \sqrt{\frac{M_{ii} + \Delta M_{ii}}{K_{ii}}}, i = 3, 4, 5 \quad (8)$$

where: ω is the natural frequency of platform motion (heave, roll or pitch) and i represents the DoF including heave, roll and pitch.

Table 5. Coupled natural frequencies of three platforms

Mode	V-shaped	OC4-DeepCWind	Braceless
Surge (rad/s)	0.054	0.058	0.079
Sway (rad/s)	0.047	0.050	0.079
Heave (rad/s)	0.250	0.360	0.240
Roll (rad/s)	0.250	0.250	0.200
Pitch (rad/s)	0.280	0.250	0.200
Yaw (rad/s)	0.092	0.075	0.110-

Comparison of hydrodynamic coefficients

This section compares the calculated hydrodynamic coefficients of the three semi platforms. Due to the symmetry, only the added mass coefficients of surge, heave and pitch are presented in Figure 3. The added mass coefficients of the OC4-DeepCwind Semi are larger than those of the other two semi platforms in heave and pitch modes (Figure 3 (b) and (c)). For lower frequencies (<1.0 rad/s), the added mass coefficients of the OC4-DeepCwind Semi in surge mode is larger than that of the other two platforms but close to that of the other two platforms in higher frequency range (>1.0 rad/s) due to the geometry of the platform.

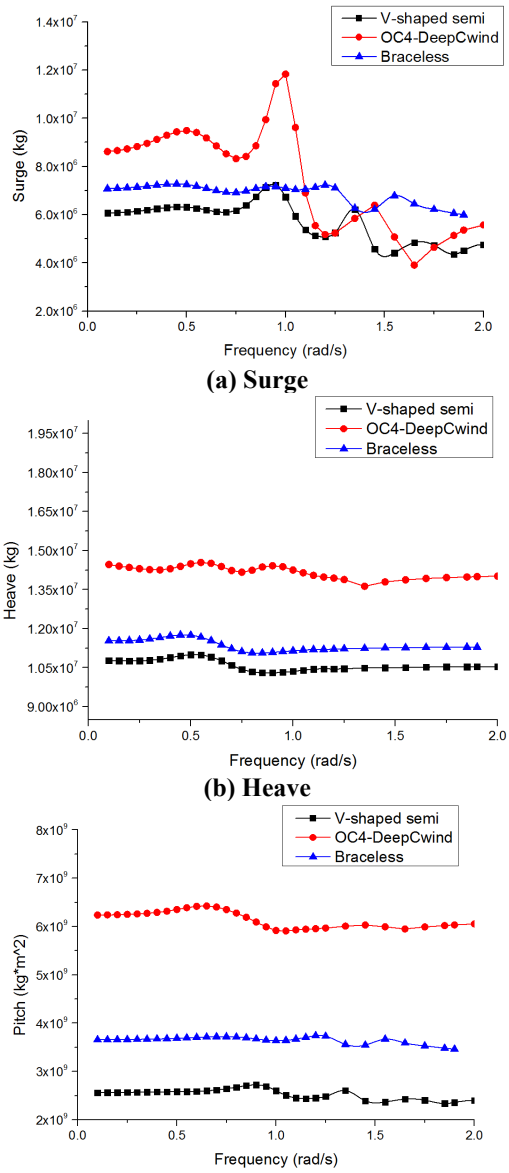

Figure 3. Added mass coefficients of the three semi platforms

The radiation damping coefficients in surge, heave and pitch are compared in Figure 4 for the examined platforms. Unlike added mass coefficients, there is no significant difference in the radiation damping due to the modes of motion. The damping coefficients of the OC4-DeepCwind Semi in surge mode are generally larger than the other two semi platforms in most of the frequency ranges while the results of the V-shaped Semi and Braceless Semi are quite similar for this mode. For lower frequencies (<1.0 rad/s), the damping coefficients of the OC4-DeepCwind Semi in heave mode are smaller than those of the other two platforms but larger than those of the other two platforms in higher frequency range (>1.0 rad/s). For pitch mode, the damping coefficients are very close to each other for the three examined semi platforms.

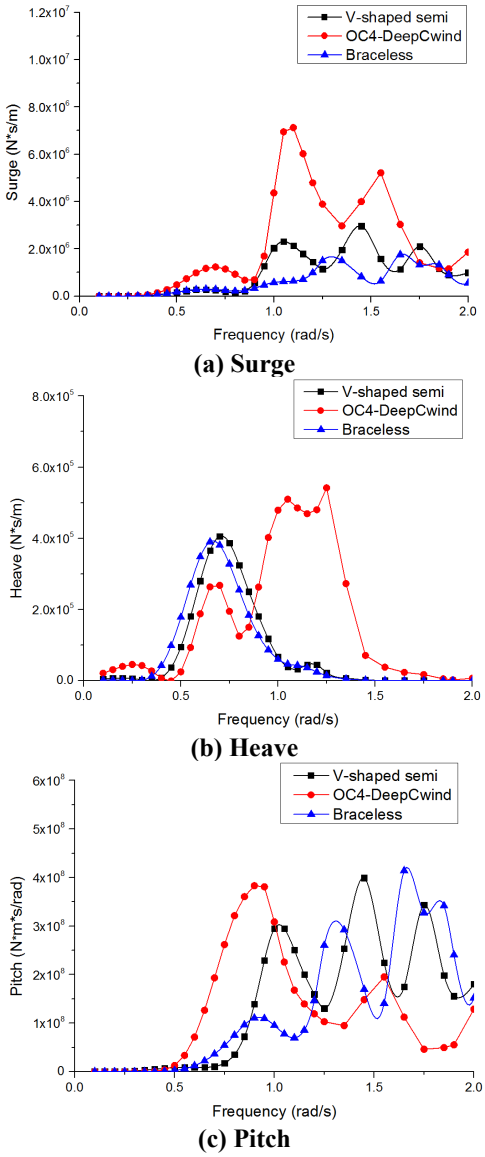

Figure 4. Radiation damping coefficients of the three semi platforms

Mooring line force-displacement relationships of the three platforms

To determine the difference in the inherent natures among the three FOWTs with different semi platforms, their force-displacement relationships are further calculated using ANSYS/AQWA (Figure 5-7). When the platform has a surge displacement, the mooring restoring load exerted on the platform increases more quickly for the OC4-DeepCwind Semi platform than the V-shaped and Braceless Semi platforms. Due to the asymmetric characteristics in the pitch direction, the pitch-pitch stiffness of the V-shaped Semi is not symmetric with respect to positive and negative pitch displacements. Furthermore, the pitch-pitch stiffness of the V-shaped Semi is less than those of the OC4-DeepCwind Semi and Braceless Semi. The heave-heave

stiffness of the Braceless Semi is less than those of the V-shaped Semi and the OC4-DeepCwind Semi, while the stiffness of the other two platforms are very similar. In addition, due to the asymmetry of the V-shaped Semi, its platform displacement in heave and roll leads to pitch restoring as well (Figure 5(b)), which is not significant for the OC4-DeepCwind Semi and Braceless Semi. This finding shows the motion coupling among those modes.

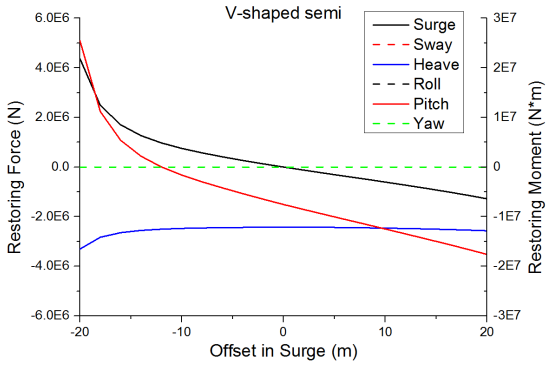

(a) Surge

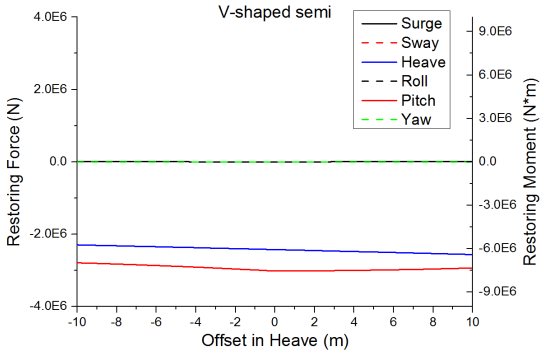

(b) Heave

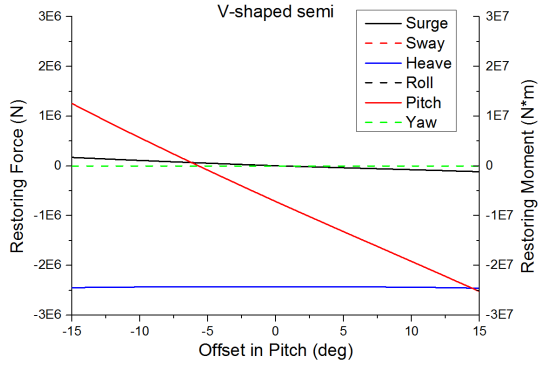

(c) Pitch

Figure 5. Load-displacement relationships for the V-shaped Semi, restoring force/moment against displacement

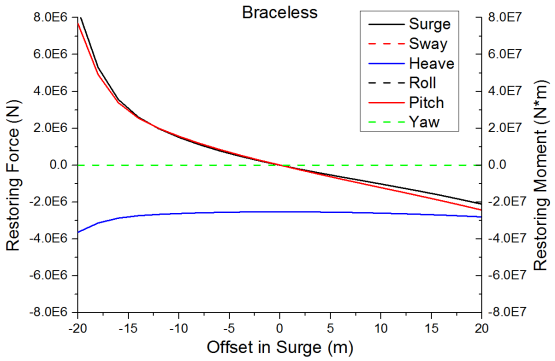

(a) Surge

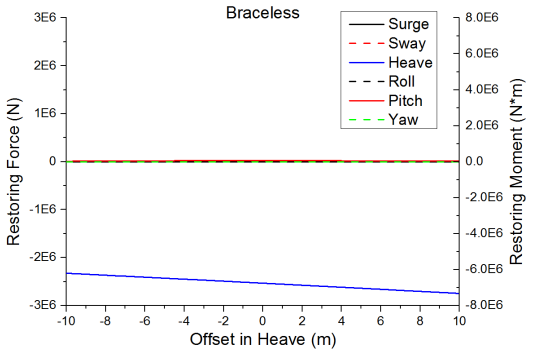

(b) Heave

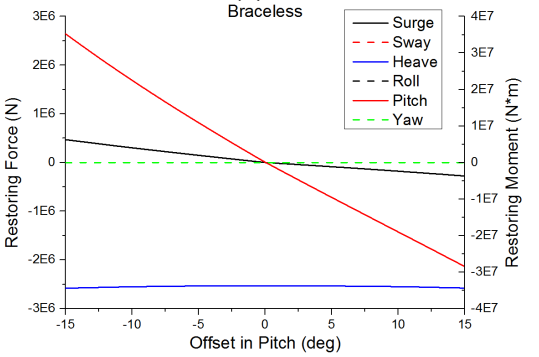

(c) Pitch

Figure 6. Load-displacement relationships for the OC4-DeepCwind Semi, restoring force/moment against displacement

Comparison of the full system response of the three FOWTs

In this section, the dynamic behavior of the three FOWTs with different semi platforms in different environmental conditions is presented. The examined load conditions represent a range of possible operational conditions according to the relevant sea conditions in the North Sea as presented in Table 4. U_w is the hub-height mean wind speed, H_s is the wave height or significant wave height and T_p is wave peak period of the JONSWAP spectrum with 3.3 of the peakedness factor that is used in order to simulate irregular waves. In this paper, both wind and waves are aligned with the mean direction that is parallel to the X-axis for all three FOWTs.

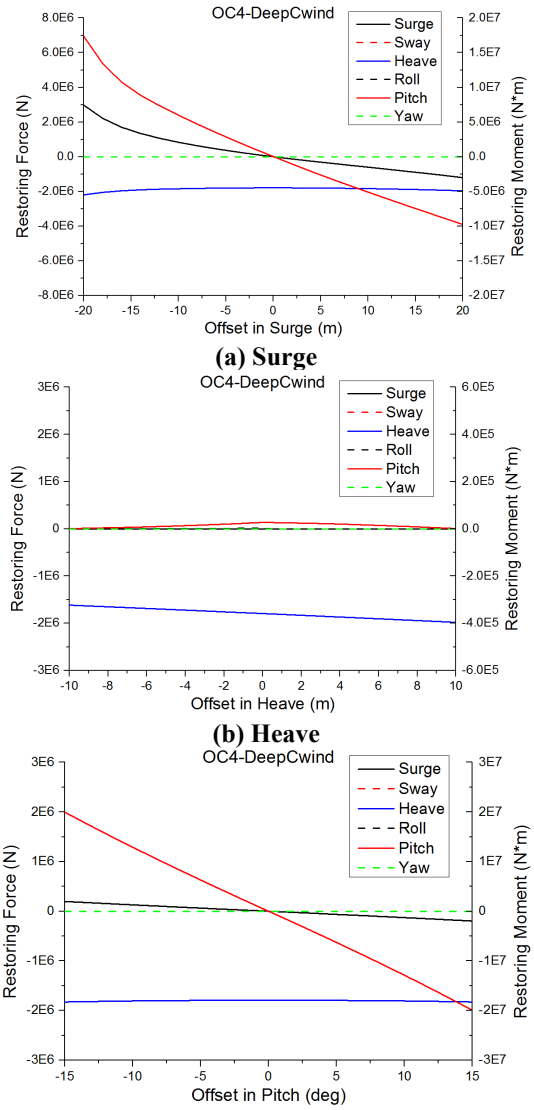

Figure 7. Load-displacement relationships for the Braceless Semi, restoring force/moment against displacement

Table 4. Load cases: LC 1, LC 2 and LC 3

Load cases	U_w (m/s)	H_s (m)	T_p (s)
LC 1	-	3.0	10.0
LC 2	8.0 (constant wind)	3.0	10.0
LC 3	49.0 (constant wind)	14.1	13.3

A moderate wave condition with wave height, H_s, 3 m and wave period, T_p, 10 s is applied to investigate the mooring system performance as well as the motion characteristics. The motion response spectrum of the three FOWTs with a 0-degree incoming wave direction in LC 1 from Table 5 is compared in Figure 8. To focus on the most critical motion response, only surge, heave and pitch motions are presented here. It must be noted that in the presented results the overall simulation time for each examined environmental condition is 4600 s, the first 1000 s have not been considered to eliminate the startup transient effects.

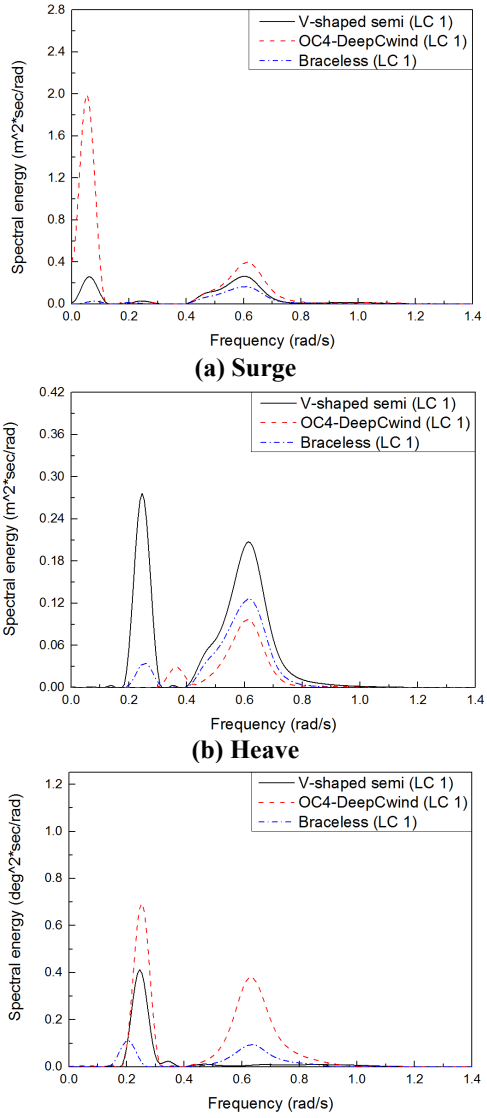

Figure 8. Motion response spectra in moderate sea state

For surge motion (Figure 8(a)), the surge resonant motion of the OC4-DeepCwind Semi is dominant at 0.058 rad/s, which is the surge natural frequency, followed by the wave frequency response in the range 0.400 rad/s to 0.800 rad/s. For the V-shaped Semi, the wave frequency response and surge resonant response are very comparable. Moreover, the coupling between the surge and pitch also contribute to the total motion response. A small peak is observed at approximately 0.200 rad/s for the Braceless Semi and 0.250 rad/s for the V-shaped Semi and the OC4-DeepCwind Semi, which coincides with the pitch resonant frequency.

For heave motion (Figure 8(b)), the wave frequency responses are also dominant in the same range for both the OC4-

DeepCwind Semi and the Braceless Semi and they are smaller than the relevant responses of the V-shaped Semi. Different from the other two semi platforms, the largest motion appears at the pitch frequency of 0.250 rad/s for the V-shaped Semi, which shows the coupling between pitch and heave for V-shaped Semi. This finding is also clearly presented in the load-displacement relationship (Figure 5 (c)).

For pitch motion (Figure 8(c)), the pitch resonant contribution is significant at 0.200 rad/s for the Braceless Semi and at 0.250 rad/s for both the V-shaped Semi and the OC4-DeepCwind Semi, which is larger than the wave frequency contribution.

The spectra for mooring lines tension in head seas for LC 1 are compared in Figure 9. For mooring line 1, which is in the downwind direction and aligns with the wind direction, the most significant contribution to the mooring line tension for the V-shaped Semi and the Braceless Semi comes from the wave frequency range from 0.400 rad/s to 0.800 rad/s, while the low-frequency response does not contribute significantly to the total response. However, the low-frequency response due to surge resonance at approximately 0.06 rad/s, for the OC4-DeepCWind, dominates the total response for mooring line 1. For mooring line 2 and 3 (results of mooring line 3 are not presented due to space limits) the contribution from the wave frequency response is in the same range as for V-shaped Semi; for the Braceless Semi is still dominating but the contribution from the surge resonance is limited.

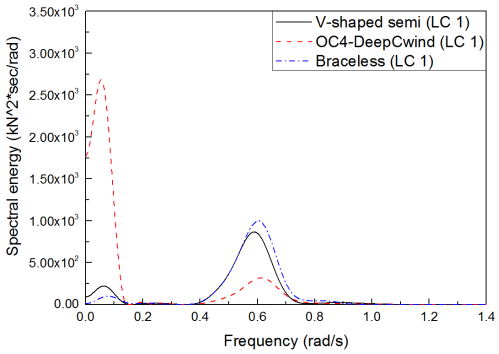

(a) Mooring line 1

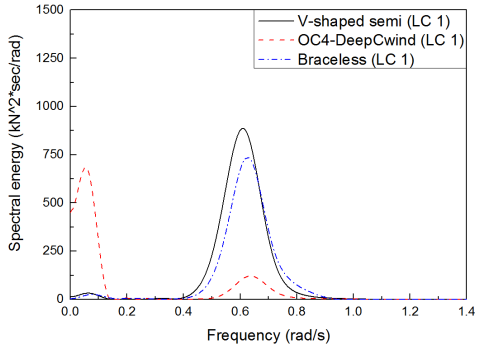

(b) Mooring line 2

Figure 9. Spectra of tension of the mooring lines in a moderate sea state

The performance of the V-shaped Semi, OC4-DeepCwind Semi and Braceless Semi subjected to environmental conditions (LC 2) corresponding to below rated wind speed and a moderate sea state is investigated in this section (Table 4). A more severe sea state with significant wave height, H_s, 3.0 m and wave peak period, T_p, 10.0 s, is used in this load case compared to LC 2.

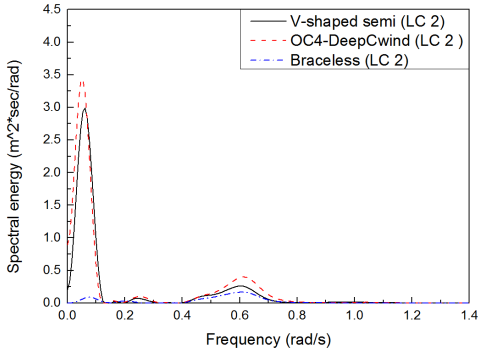

(a) Surge

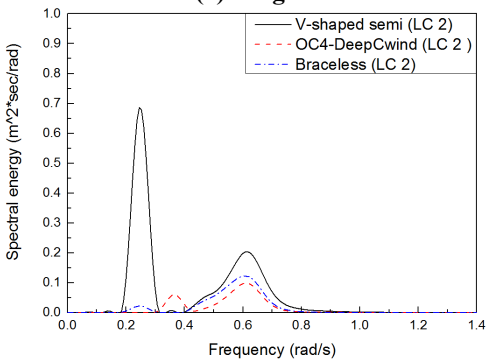

(b) Heave

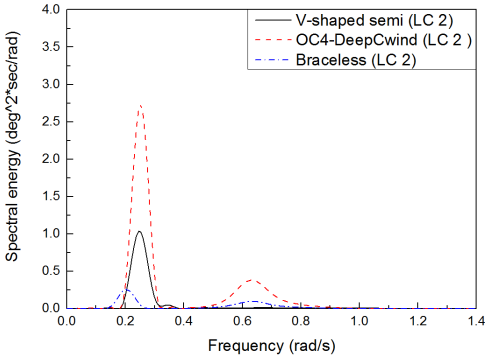

(c) Pitch

Figure 10. Motion response spectra in a moderate sea state including wind condition

For surge motion (Figure 10(a)), the contribution from the surge resonant motion to the V-shaped Semi, OC4-DeepCwind Semi, and Braceless Semi are similar to LC 1 but exhibits a large increase in the total response due to wind load and severe wave condition is occurred. Comparing LC 1 and LC 2, it finds that the wind load does not influence the wave frequency region. However, it will contribute to resonant response frequencies at

low-frequency regions such as surge, heave and pitch natural frequencies.

For heave motion (Figure 10(b)), the wave frequency responses are also dominant in the same frequency range for the V-shaped Semi and Braceless Semi. However, the pitch resonant motion provides a large contribution to the total response of the V-shaped Semi due to the coupling of the modes. For the OC4-DeepCwind Semi, the heave resonance shows the largest contribution to the total motion response followed by the wave resonant response.

For pitch motion (Figure 10(c)), the pitch resonant contribution dominates the total response at 0.250 rad/s for the OC4-DeepCwind Semi. Larger total motion response can be found for all three platforms due to the wind force when compared to LC 1.

The spectra for mooring line tensions in the head sea for LC 2 are presented in Figure 11. For mooring line 1, the wave frequency response of the V-shaped Semi and Braceless Semi is dominated in the range between 0.400 rad/s to 0.800 rad/s followed by the surge resonant motion around 0.060 rad/s. However, for the OC4-DeepCwind Semi, the most significant contribution to the mooring line tension comes from the surge resonant response. This contribution is similar to the case of mooring line 2.

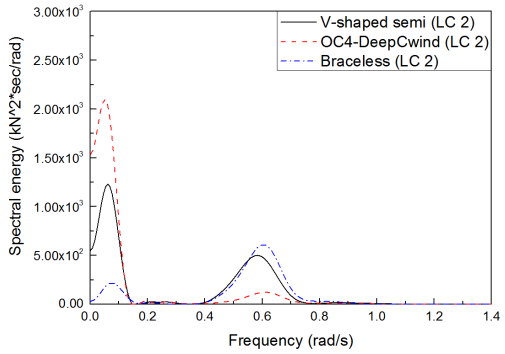

(a) Mooring line 1

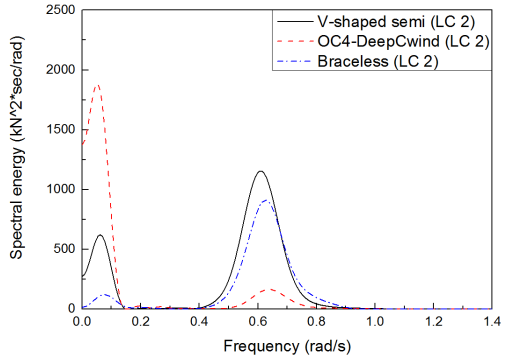

(b) Mooring line 2

Figure 11. Spectra of the tension of mooring lines in a moderate sea state including wind condition

The performance of the V-shaped Semi, OC4-DeepCwind Semi and Braceless Semi subjected to extreme environmental conditions (LC 3) are investigated in this section. A 50-year reoccurrence of extreme wind condition with a wind speed of 49.0 m/s, and extreme wave condition with a significant wave height, H_s, 14.1 m and wave peak period, T_p, 13.3 s is adopted from a specific offshore site in the North Sea off the Norwegian coast. The motion response spectra of surge, heave and pitch for heading wave are presented in Figure 12.

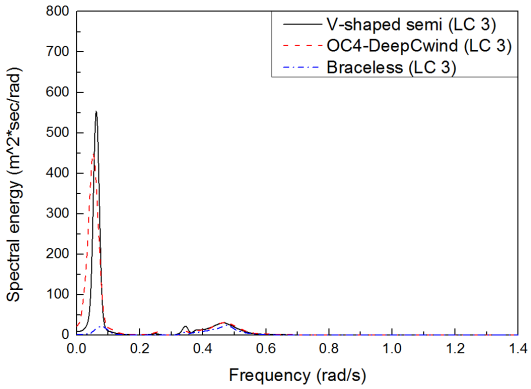

(a) Surge

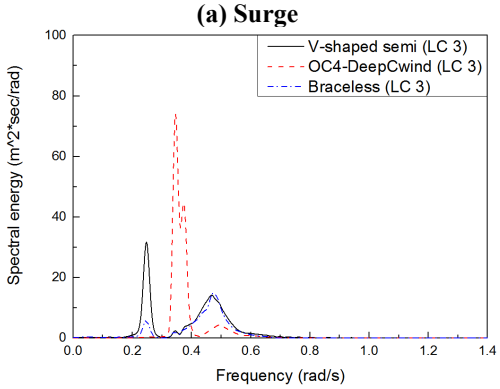

(b) Heave

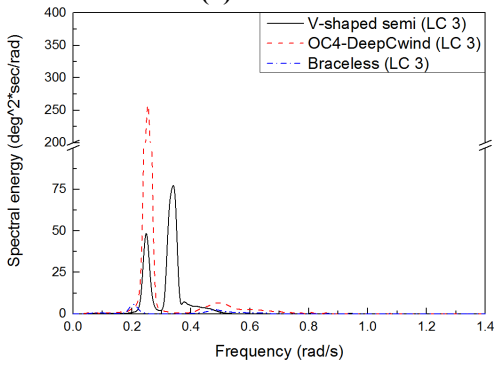

(c) Pitch

Figure 12. Motion response spectra in an extreme sea state

For surge motion (Figure 12(a)), the surge resonant response is dominant since the wave-frequency response doesn't contribute too much to the total response of the V-shaped Semi and the OC4-DeepCwind Semi. The contribution from the surge resonance frequency and wave frequency to the total response of the Braceless Semi under this load case are very comparable. For

heave motion (Figure 12(b)), the wave frequency responses are also dominant in the same range for the Braceless Semi. However, the pitch resonant motion gives a large contribution to the total response of the V-shaped Semi due to the coupling of the modes. For the OC4-DeepCwind Semi, the heave resonance frequency shows a significant contribution to the total motion response. For pitch motion (Figure 12(c)), the pitch resonant contribution dominates the total response at 0.250 rad/s for the OC4-DeepCwind Semi. For the Braceless Semi, the contribution from the surge resonance frequency and wave frequency to the total response of the Braceless Semi are very comparable. However, both the pitch resonant response and the heave resonant response dominate the motion response of the V-shaped Semi. The mode coupling effect is significant for the V-shaped Semi. The spectra for the mooring lines tension in the extreme sea state for LC 3 are presented in Figure 13. For mooring line 1, the wave frequency response of the Braceless Semi is dominated in the range between 0.400 rad/s to 0.800 rad/s, which is significantly larger than the surge resonant motion at approximately 0.060 rad/s. However, for the OC4-DeepCwind Semi, the most significant contribution to the mooring line tension comes from the surge resonant response followed by wave frequency response. However, the contribution to the response of the mooring line from the wave frequency and the surge resonance for the V-shaped Semi are quite comparable. A similar observation is met for the case of mooring line 2.

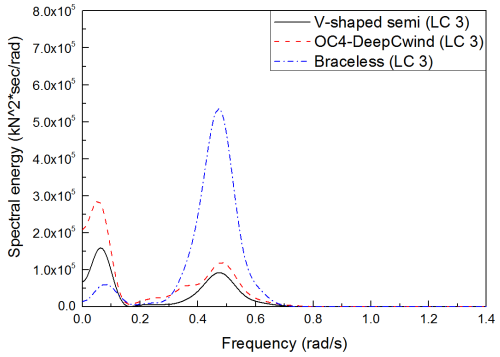

(a) Mooring line 1

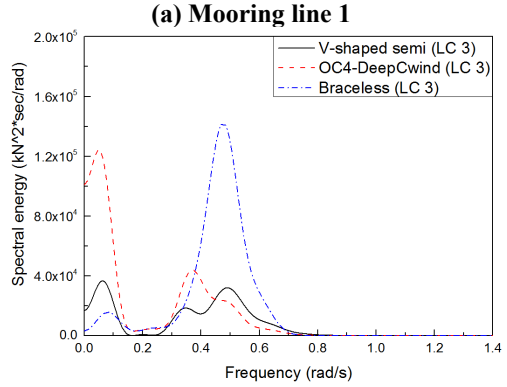

(b) Mooring line 2

Figure 13. Spectra of tension of mooring lines in an extreme sea state

CONCLUSIONS

In the present paper, a comparison between three FOWTs, namely, V-shaped Semi, OC4-DeepCwind Semi and Braceless Semi platforms is presented. The dynamic response analysis and performance of the FOWTs under wind and wave loads is investigated. An extensive discussion has been made and useful conclusions can be summarized into the following aspects: 1) The V-shaped Semi and the Braceless Semi show a more rational dynamic motion response under the load cases investigated in this work when compared to the OC4-DeepCwind Semi. However, the spectrum of mooring line tension of the V-shaped semi and Braceless Semi has larger wave-frequency components since the peak of the wave frequency is larger than the motion natural frequency in PSD plots. 2) The motion coupling effect is very significant for the V-shaped Semi platform due to its asymmetric geometry. Specific attention should be paid to this design due to the heave mode and pitch mode coupling. 3) The natural frequency of the OC4-DeepCwind in heave motion is approximately 0.360 rad/s which is close to the range of the wave frequency. This could cause great resonance and threaten the safety of the structures. The natural frequency should be further considered to prevent it from approaching the range of the wave frequency.

ACKNOWLEDGEMENT

The authors would like to gratefully acknowledge financial support from the National Natural Science Foundation of China (Grant No. 51709039, 51709040). This work is partially supported by the international collaboration and exchange program from the NSFC-RCUK/EPSRC with grant No. 51761135011.

REFERENCES

[1] Remy, T., and Mbistrova, A., 2018. Offshore Wind in Europe: Key Trends and Statistics 2017. Wind Europe: Brussels, Belgium,.

[2] Shi, W., Tan, X., Gao, Z., and Moan, T., 2016. Numerical study of ice-induced loads and responses of a monopile-type offshore wind turbine in parked and operating conditions. Cold Regions Science and Technology, 123, 121-139.

[3] Jiang, Z., Moan, T., and Gao, Z., 2015. A comparative study of shutdown procedures on the dynamic responses of wind turbines. Journal of Offshore Mechanics and Arctic Engineering, 137(1), 011904.

[4] Shi, W., Park, H.C., Chung, C.W., Shin, H.K., Kim, S.H., Lee, S.S., and Kim, C.W., 2015. Soil-structure interaction on the response of jacket-type offshore wind turbine. International Journal of Precision Engineering and Manufacturing-Green Technology, 2(2), 139-148.

[5] Jiang, Z., Li, L., Gao, Z., Halse, K. H., and Sandvik, P. C., 2018. Dynamic response analysis of a catamaran installation vessel during the positioning of a wind turbine assembly onto a spar foundation. Marine Structures, 61, 1-24.

[6] Bachynski, E.E.; Eliassen, Lene. (2018) The effects of coherent structures on the global response of floating

offshore wind turbines. Wind Energy, https://doi.org/10.1002/we.2280.
[7] Ren, Z., Jiang, Z., Skjetne, R., and Gao, Z., 2018. An active tugger line force control method for single blade installations. Wind Energy, 21:1344–1358.
[8] Roddier, D., Peiffer, A., Aubault, A., and Weinstein, J., 2011. A generic 5 MW WINDFLOAT for numerical tool validation & comparison against a generic spar. ASME 2011 30th International Conference on Ocean, Offshore and Arctic Engineering, Rotterdam, The Netherlands, June 19–24.
[9] Ishihara, T., 2013. Fukushima FORWARD, Fukushima Offshore Wind Consortium, http://www.fukushima-forward.jp/english/index.html.
[10] Landbø, T., 2013. OO Star Wind Floater: A robust and flexible concept for floating wind. Norway, Dr. techn. Olav Olsen.
[11] Bayati, I., Jonkman, J. and Robertson, A., 2014. The effects of second-order hydrodynamics on a semisubmersible floating offshore wind turbine, Journal of Physics: Conference Series, 524(1), 1-10.
[12] Masciola, M., Robertson, A., Jonkman, J., Coulling, A., & Goupee, A., 2013. Assessment of the importance of mooring dynamics on the global response of the DeepCwind floating semisubmersible offshore wind turbine. Proc 23rd International Offshore and Polar Engineering Conference, Anchorage, Alaska, ISOPE
[13] Luan, C., Gao, Z. and Moan, T., 2016. Design and Analysis of a Braceless Steel 5-MW Semi-Submersible Wind Turbine, Proc 35th International Conference on Ocean, Offshore and Arctic Engineering, American, ASME, 1-12.
[14] Michailides C., Gao Z. and Moan T., 2016. Experimental Study of the Functionality of a Semisubmersible Wind Turbine Combined with Flap-Type Wave Energy Converters. Renewable Energy, 93, 675-690.
[15] Michailides, C., Gao, Z. and Moan, T., 2016. Experimental and numerical study of the response of the offshore combined wind/wave energy concept SFC in extreme environmental conditions. Marine Structures, 50, 35-54.
[16] Kim, H.C., Kim, M.H. and Lee, J.Y., 2017. Global performance analysis of 5MW WindFloat and OC4 Semisubmersible floating offshore wind turbines(FOWT) by numerical simulations, Proc 27th International Offshore and Polar Engineering Conference, San Franciso, ISOPE, 546-553
[17] Jonkman J. and Buhl M.L., 2005. FAST User's Guide.
[18] Manwell J.F., McGowan J.G., and Rogers A.L., Wind Energy Explained. England: John Wiley & Sons; 2004.
[19] Jonkman, J., Butterfield, S., Musial, W., Scott, G., 2009. Definition of a 5-MW reference wind turbine for offshore system development. Golden, CO, National Renewable Energy Laboratory. NREL Report TP-500-38060.
[20] Matha, D., Schlipf, M., Pereira, R., and Jonkman, J., 2011. Challenges in simulation of aerodynamics, hydrodynamics, and mooring-line dynamics of floating offshore wind turbines. Proc 21st International Offshore and Polar Engineering Conference, Hawaii, ISOPE.
[21] Karimirad, M., and Michailides, C., 2015. V-shaped Semisubmersible offshore wind turbine: An alternative concept for offshore wind technology. Renewable Energy, 83, 126-143.
[22] Michailides, C., and Karimirad, M., 2015. Mooring System Design and Classification of an Innovative Offshore Wind Turbine in Different Water Depth. Recent Patents on Engineering, 9(2), 104-112.
[23] Karimirad, M. and Michailides, C., 2016. V-shaped Semi-submersible Offshore Wind Turbine Subjected to Misaligned Wave and Wind. Journal of Renewable and Sustainable Energy, 8(2), 023305-1-023305-17.
[24] Robertson, A., Jonkman, J., Vorpahl, F., Popko, W., Qvist, J., Frøyd, L., et al, 2014. Offshore code comparison collaboration continuation within IEA wind task 30: phase II results regarding a floating semisubmersible wind system. In ASME 2014 33rd International Conference on Ocean, Offshore and Arctic Engineering (pp. V09BT09A012-V09BT09A012). American Society of Mechanical Engineers.